Intermediate-coupling calculation of atomic spectra from hot plasma

A. Goldberg, B. F. Rozsnyai, and P. Thompson
Lawrence Livermore National Laboratory, University of California, P.O. Box 808, Livermore, California 94550
(Received 25 February 1985; revised manuscript received 4 February 1986)

An algorithm is presented for the detailed computation of the spectral lines in hot, partially ionized plasmas in local thermodynamic equilibrium. The procedure uses the wave functions and state probabilities determined from the average atom model for microscopic configuration accounting. We use intermediate coupling to include the detailed structure of the bound-bound transition arrays. The model is applied to bromine plasma under such temperature and density conditions that partially filled L shells occur.

I. INTRODUCTION

The proper accounting of the large number of spectral lines in hot, partially ionized matter is important for opacities and also for plasma diagnostics. Teller[1] first recognized the importance of line opacities in hot matter, subsequently rediscovered by many other researchers. The strong effect of dispersed line clusters on the Rosseland mean opacity of partially ionized gold was demonstrated by Nardi and Zinamon.[2] A brief quantitative illustration of the relative importance of line and continuum opacities for iron plasma was also given by Rozsnyai.[3] Theoretical estimates for the degree of dispersion of line clusters due to the different angular momentum states of the many-electron system were given by Moszkowski,[4] and more recently in a series of reports by Bauche *et al.*[5-7]

Although the estimate of the degree of dispersion of lines due to the different angular momentum states is important, a detailed accounting of lines is necessary for accurate opacity calculations and also to predict expected spectral patterns. Whether or not the line clusters actually merge into continuous profiles depends on the physical line-broadening characteristics of the plasma, so that line broadening is an integral part of the spectroscopic model. The main objective of this paper is to describe a computational procedure for the accounting of the large number of spectral lines in medium-Z plasmas at temperatures such that partial ionization occurs. Since the computation problem is enormous, approximations are a practical necessity. Presently we use first-order perturbation theory for the computation of spectroscopic terms. The spin-orbit interaction is taken into account in our model Hamiltonian and we use the intermediate coupling scheme, so that our model is applicable for high-Z elements. We present some calculations for bromine plasma at temperatures and densities corresponding to partially filled L shells. For the present, we limit our model to conditions of local thermodynamic equilibrium (LTE). In Sec. II we present the theoretical basis of our model and in Sec. III we present some computational results.

II. THEORY

The theoretical basis of our model is the utilization of the "average atom" (AA) wave functions to compute the expectation values of our model Hamiltonian. These expectation values are computed for eigenstates of the J^2 operator of the many-electron system. The AA model, which is the starting point of our computational procedure, is described by Rozsnyai,[8] and in references given there; here we merely recall the rudiments of that model.

The AA model assumes that the electronic levels in the plasma are populated according to the Fermi statistics

$$q_{nl}=g_{nl}\{\exp[-(\varepsilon_{nl}-\mu)/kT]+1\}^{-1}\ , \tag{1}$$

where q_{nl} and g_{nl} are the population and statistical weight of a single particle level ε_{nl} with quantum numbers n and l, μ is the Fermi level, and kT is the temperature in energy units. The electronic potential is assumed to be spherically symmetry and the radial part of the single particle wave functions satisfy Schrödinger's equation (in atomic units)

$$R''_{nl}+2R'_{nl}/r+\{2[\varepsilon_{nl}-V(r)]-l(l+1)/r^2\}R_{nl}=0\ . \tag{2}$$

In Eq. (2) the electronic potential is given by

$$V(r)=-Ze^2/r+e^2\int d^3r'\frac{\rho(r')}{|\mathbf{r}-\mathbf{r}'|}+V_{\rm xc}[\rho(r)]\ , \tag{3}$$

where Z stands for the charge of the nucleus and the electron density is given by

$$\rho(r)=\sum_{n,l}q_{nl}\,|\,R_{nl}(r)\,|^2\ . \tag{4}$$

The last term in Eq. (3) stands for the exchange-correlation part, approximated by a local potential which is a unique functional of the electron density. In our model for $V_{\rm xc}$ we adopt the formula of Hedin and Lundqvist.[9]

It should be noted that in Eq. (4) the summation goes over all states, including the continuum. Because of that, our model includes the screening effect by the continuum electrons also. The actual computational technique to account for the free electrons is described in Ref. 8.

For a given temperature the Fermi level μ is determined by the condition of charge neutrality

$$\int_0^{r_0}\rho(r)r^2\,dr=Z\ , \tag{5}$$

where r_0 stands for the ion sphere radius determined by

the matter density.

Equations (1)—(5) give a complete self-consistent set of equations for the AA model. The model's shortcoming is that at finite temperature it predicts noninteger occupation numbers for the electronic levels, making the physical state of the AA fictitious. The usefulness of the AA model extends to the degree of its usefulness as a statistical average.

We proceed by separating the electronic levels of the AA into core and valence states. Core states are those for which $q_{nl} \sim g_{nl}$, which is the case for energy levels well below the Fermi level. Valence states are those with fractional or near zero occupational numbers. We create concrete physical electronic states involving the valence states in the following manner.

First, we truncate the AA occupational numbers to their nearest integer values creating the "most probable atom." In contrast to the AA, the most probable atom is not fictitious but a physically permissible specimen. Next, we create different electronic configurations from the most probable atom by promoting and demoting electrons in the valence levels. We also create different charge states by increasing or decreasing the number of valence electrons and repeating the same procedure. For each configuration we create all the possible combinations for the lowest value of J_z. We use this set to simultaneously diagonalize the J^2 operator and the Hamiltonian for the valence electrons. Since we are faced with an enormous number of possible states we restrict ourselves to those with appreciable probability. The procedure described above is carried out for the "parent" and "daughter" configurations. Parent and daughter configurations are distinguished by promoting an electron from an nl state to an upper $n'l'$ state due to photoabsorption. A somewhat similar calculational method has been given by Argo and Huebner,[10] where the energies of the angular momentum states were not resolved, and also the configurational energies utilized Slater integrals Z scaled for isolated ions. More recently Goldberg and Rozsnyai[11] gave results from a simplified version of the model described in this paper where only the lower parent configurations were energy resolved.

Our model Hamiltonian used for the computation of term energies and for the probabilities of the parent states is given by

$$H = H_0 + \tfrac{1}{2} \sum_{i,j} \frac{e^2}{|\mathbf{r}_i - \mathbf{r}_j|} + \frac{\hbar^2}{4m^2c^2} \sum_i \frac{1}{r_i} \frac{dV_{AA}(r_i)}{dr_i} \mathbf{l}_i \cdot \mathbf{s}_i \,, \tag{6}$$

with i and j covering the valence electrons only, and

$$H_0 = \sum_i \left[-\frac{\hbar^2}{2m} \nabla_i^2 - \frac{Ze^2}{r_i} + V_c(r_i) \right] . \tag{7}$$

The term V_c in Eq. (7) stands for the "core" potential due to the charge distribution of the core electrons, and is given by

$$V_c(r) = \int d^3r' \rho_c(r') \frac{e^2}{|\mathbf{r} - \mathbf{r}'|} + V_{xc}[\rho_c(r)] \,, \tag{8}$$

with

$$\rho_c(r) = \sum_c q_{nl} |R_{nl}(r)|^2$$

and the summation goes over the core states. The spin-orbit interaction in Eq. (6) is taken into account in the AA approximation to the degree that $V_{AA}(r_i)$ stands for the AA one-electron potential. We compute the expectation values of the Hamiltonian (6) for all parent and daughter states which are eigenstates of the J^2 operator. Since the Hamiltonian (6) involves the valence electrons only, the self-energy of the core is unaccounted for. For the computation of transition energies between parent and daughter states due to photoabsorption the core self-energy cancels out to the extent that core polarization and relaxation are negligible.

We thus construct linear combinations of Slater determinental wave functions, the determinants comprised of the single-particle orbitals for the valence electrons. These linear combinations are chosen to simultaneously diagonalize $J^2 = (\sum \mathbf{J})^2$, and H [Eq. (6)], within the subspace of one configuration, where of course the sums are taken over the valence electrons only. This diagonalization is performed directly and does not utilize tables of fractional parentage coefficients.

If we label the expectation value of the Hamiltonian (6) for a J state in a certain configuration α by $E(J,\alpha)$, then the probability of that state under LTE condition is given by

$$P(J,\alpha) = KG(J) \exp\{-[E(J,\alpha) - \mu N_v]/kT\} \,, \tag{9}$$

where N_v is the number of valence electrons in the configuration α. In Eq. (9), $G(J)$ is the statistical weight $(2J+1)$ and the constant K is determined by the normalization condition

$$\sum_{J,\alpha} P(J,\alpha) = 1 \,.$$

Our aim is to account for all the absorption lines of a cluster associated with a single-electron transition of the type $nl - n'l'$ ($n < n'$ and $l = l' \pm 1$) where the members of a cluster differ by belonging to different parent configurations and/or J states. The transition energy of a particular line is

$$\Delta E = E(J',\alpha') - E(J,\alpha) \,, \tag{10}$$

with the selection rule $\Delta J = 0, \pm 1$, (no 0-0 transitions) and where the configurations differ by one in the occupation number of the one-electron states $nl, n'l'$. To obtain the desired spectra we have computed all the relevant term energies and oscillator strengths for all the transitions of the type in Eq. (10), together with the probabilities of the parent states as given by Eq. (9).

The oscillator strengths and term energies are calculated using the AA wave functions as the basis single-particle set for our many-body representation. In this sense our model is a first-order perturbation calculation using the self-consistent AA model as a start.

In order to obtain a meaningful spectroscopic result the bound-bound oscillator strengths have to be supplied with

reasonable line-shape profiles to compute frequency-dependent absorption cross sections. In a real plasma the bound-bound cross sections are superimposed on the bound-free and free-free, which also have to be taken into account. The computation of spectrum profiles, bound-free and free-free processes is described by Rozsnyai[12–15] and the reader is referred to the quoted references. In the next section we illustrate our model by presenting some calculations for bromine plasma

III. NUMERICAL CALCULATIONS

We apply the procedure described in Sec. II to the partially filled L shell for the bromine plasma. At present no experimental data for LTE plasmas are known to the authors. In the case of laser or electron-beam-produced plasmas only the free electrons, which are usually Maxwellian, have the property of a temperature, and the bound electrons over the ions are distributed according to the collision-radiative rate equations. Therefore, it is rather difficult to correlate our LTE model with the available experimental data. Nevertheless, we attempt to do that by choosing the temperature-density conditions so that the LTE distribution of the different ionic species is close to those of the non-LTE experimental conditions. In Fig. 1 we show the experimental measurements of Bailey *et al.*[16] for laser-produced bromine plasma. The free-electron density and temperature were estimated as 5×10^{21} cm^{-3} and 480 eV, respectively, and the plasma is mainly neon- and fluorine-like and optically thin. In order to check the accuracy of our computed transition energies, we have marked in Fig. 1 some of the prominent neon and fluorinelike lines, and we have also listed them in Table I. To mimic the experimental conditions with our LTE model, we chose the same electron density, corresponding to 2.6×10^{-2} matter density, and to make the plasma mainly neon- and fluorine-like, we had to take the temperature as 270 eV. In this case the AA model predicts an almost filled L shell corresponding to fluorinelike configurations. In our detailed configuration accounting we include 12 parent configurations, with the neon-, fluorine-, and oxygen-like states having the largest probability, giving rise to 54 initial J states. For these 54 parent states we accounted for all the $n=2$-3, 2-4, and 2-5 transitions in the intermediate-coupling approximation,

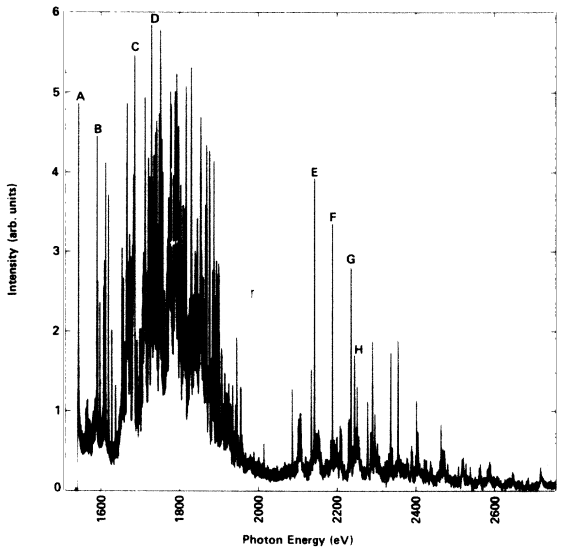

FIG. 1. Experimental measurement of photoemission (in arbitrary units) from a bromine plasma with 5×10^{21} cm^{-3} free-electron density and 480 eV free-electron temperature. Details are given in Ref. 17. The lines marked by the capital letters are listed in Table I.

which yielded 10 632 spectral lines. We list the parent configurations together with the number of J states and parent-state probabilities $\sum_J P(J,\alpha)$ in Table II, and show the oscillator strengths multiplied by the probabilities of the parent states leading to the $nl-n'l'$ transition arrays in Figs. 2 and 3. We supply the lines with reasonable line-shape profiles and, having computed the bound-free and free-free absorption cross sections as described in Refs. 11–14, we then compute the total photoabsorption cross section for the plasma. We predict the emission spectrum from the plasma by taking the simplest solution of the radiative-transfer equation

$$I(\nu)=B(\nu)\{1-\exp[-\sigma(\nu)\rho L]\}\ , \tag{11}$$

where $I(\nu)$ is the intensity of the emerging radiation, $B(\nu)$ is the Planck function, $\sigma(\nu)$ the frequency-dependent photoabsorption cross section, ρ is the matter density and L is the average distance inside of the plasma

TABLE I. Some of the outstanding lines of Figs. 1 and 6. The parent configurations, single-electron $j-j'$ and many-electron $J-J'$ transitions are listed in columns 2, 3, and 4. The transition energies are given in electron volts. The numbers in square brackets are exponents of 10.

Line	Par. Conf.	$j-j'$ transitions	$J-J'$ transitions	ΔE (calc.)	ΔE (meas.)
A	[Ne]	$2p_{3/2}$-$3s_{1/2}$	0-1	1.536[3]	1.543[3]
B	[Ne]	$2p_{1/2}$-$3s_{1/2}$	0-1	1.563[3]	1.591[3]
C	[Ne]	$2p_{3/2}$-$3d_{5/2}$	0-1	1.685[3]	1.685[3]
D	[Ne]	$2p_{1/2}$-$3d_{3/2}$	0-1	1.716[3]	1.728[3]
E	[Ne]	$2p_{3/2}$-$4d_{5/2}$	0-1	2.143[3]	2.145[3]
F	[Ne]	$2p_{1/2}$-$4d_{3/2}$	0-1	2.167[3]	2.191[3]
G	[F]	$2p_{3/2}$-$4d_{5/2}$	$\frac{3}{2}$-$\frac{5}{2}$	2.240[3]	2.234[3]
H	[F]	$2p_{1/2}$-$4d_{3/2}$	$\frac{1}{2}$-$\frac{3}{2}$	2.249[3]	2.243[3]

TABLE II. Parent configurations, number of J states and probabilities for bromine plasma at $kT=270$ eV and at $\rho=2.6\times10^{-2}$ g/cm^3. The numbers in square brackets are exponents of 10.

Configuration	No. of J states	$\sum_J P(J,\alpha)$
[Na]	1	8.504[−3]
[He]$2s^2 2p^5 3s^1$	4	9.011[−3]
[Ne]	1	3.095[−1]
[He]$2s^1 2p^6$	1	6.086[−2]
[He]$2s^2 2p^4 3s^1$	8	3.951[−3]
[F]	2	3.269[−1]
[He]$2s^1 2p^5$	4	6.427[−2]
[O]	5	1.438[−1]
[He]$2s^1 2p^4$	8	2.828[−2]
[N]	5	3.375[−2]
[He]$2s^1 2p^3$	10	6.635[−3]
[C]	5	4.455[−3]

material through which the photons must pass before emerging and reaching the detector. We show our computed photoabsorption cross sections in Figs. 4 and 5, and the calculated emission spectrum using Eq. (11) in Fig. 6. The emission intensity in Fig. 6 is on the linear scale to compare our data with experimental measurements. We choose the sample thickness L to be 2.5×10^{-3} cm, corresponding to the experimental conditions.

A comparison of Figs. 1 and 6, as well as inspection of Table I shows that the calculated strong lines have about the same transition energies as those of the experiment. However, the strength ratios seem to be different. We have no explanation for this difference beyond the suspicion that it is due to the difference between the LTE model and non-LTE experimental conditions. Presently we have no experimental data to compare our calculations with experiments where LTE conditions exist.

In Table III we compare briefly the data predicted by the AA model with those of our detailed spectroscopic ac-

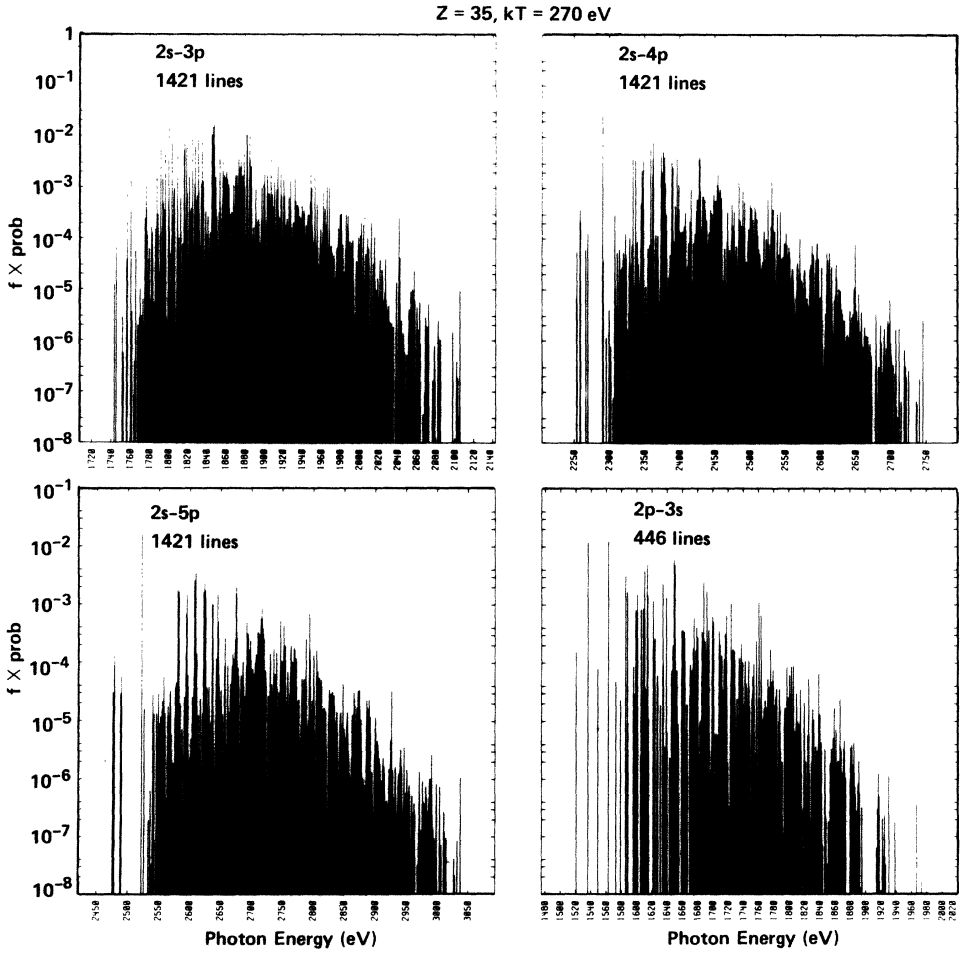

FIG. 2. Computer output for the $2s$-$3p$, $2s$-$4p$, $2s$-$5p$, and $2p$-$3s$ transition arrays vs photon energy in eV for bromine plasma at $kT=270$ eV and at $\rho=2.6\times10^{-2}$ g/cm^3. The vertical scale is for the oscillator strengths multiplied by the probability of the parent state.

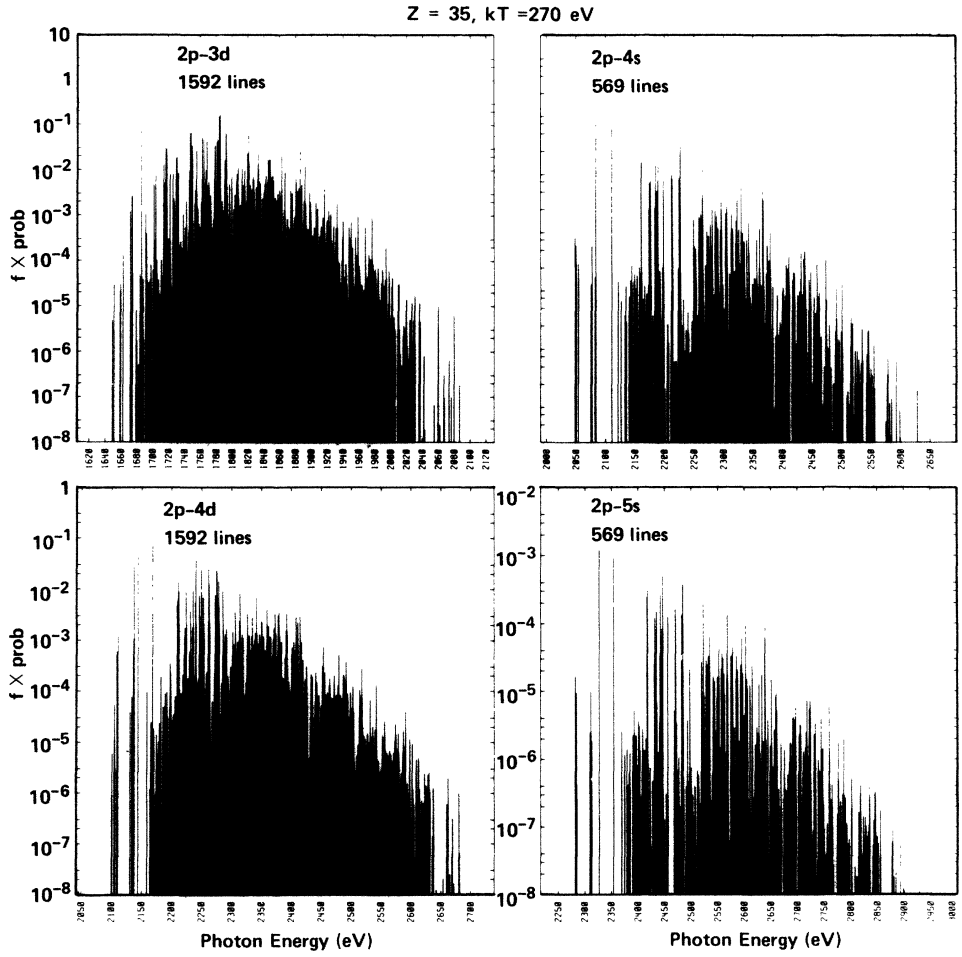

FIG. 3. Same as Fig. 2 for the $2p$-$3d$, $2p$-$4s$, $2p$-$4d$, and $2p$-$5s$ arrays.

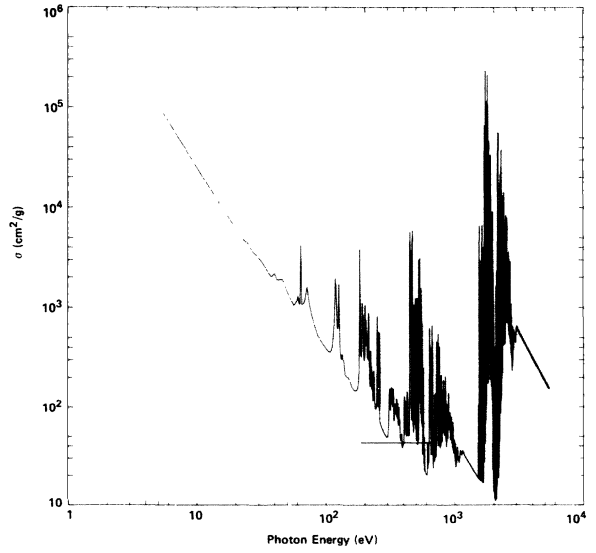

FIG. 4. Calculated total photoabsorption cross section in units of cm^2/g versus photon energy for bromine at $kT=270$ eV and at $\rho=2.6\times10^{-2}$ g/cm.

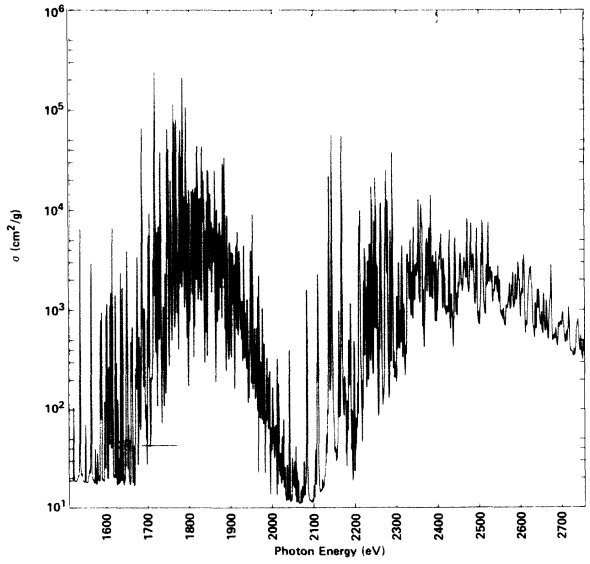

FIG. 5. Same as Fig. 4 over the smaller photon energy range of 1500—2800 eV corresponding to experimental measurements.

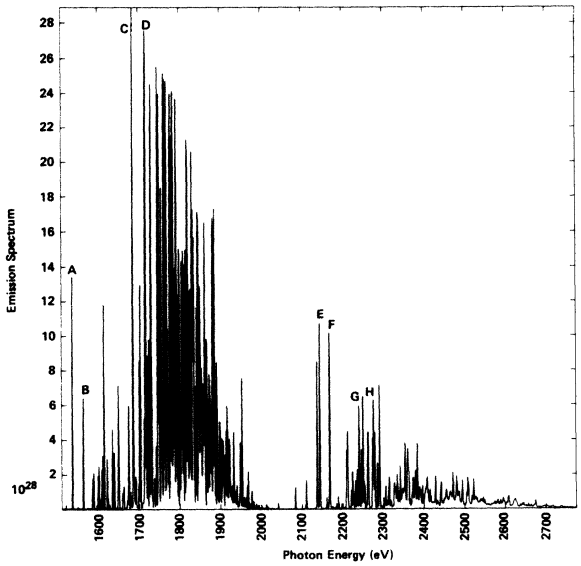

FIG. 6. Calculated emission spectrum in units of the Planckian function $B(\nu)$ for bromine plasma using the photoabsorption cross section of Fig. 5 ($kT=270$ eV and $\rho=2.6\times10^{-2}$ g/cm^3) and a sample thickness of 2.5×10^{-3} cm. The letters indicate the lines listed in Table I.

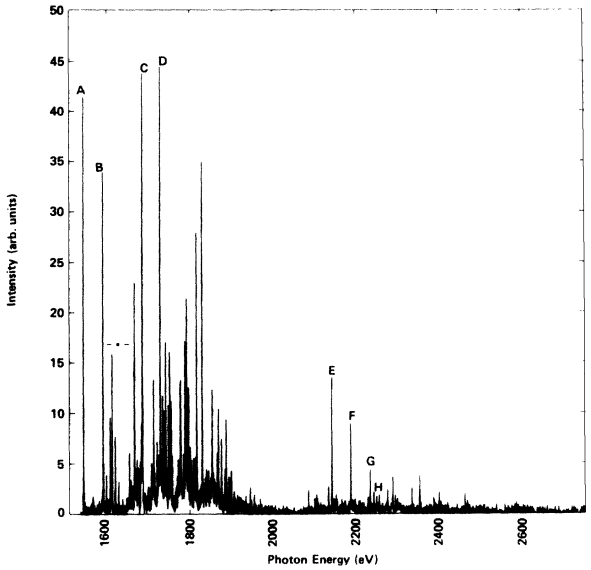

FIG. 7. Same as Fig. 6 for 3×10^{21} free-electron density and 710 eV free-electron temperature. The asterisk indicates the region of the F-like $2p$-$3s$ transitions.

counting. In column 2 the transition energy $\Delta E(aa)$ is simply the difference of the single particle energy levels as predicted by the self-consistent AA model. In column 3 $\Delta E(a)$ is the average transition energy of a $nl-n'l'$ array given by

$$\Delta E_{nl-n'l'}(a)=\sum_{\lambda,\lambda'} P(\lambda)f(\lambda\rightarrow\lambda')\Delta E(\lambda\rightarrow\lambda')f^{-1}_{nl\rightarrow n'l'}(a)\ , \tag{12}$$

where the summation goes over all the parent J states labeled by λ and over all the daughter J' states labeled by λ' which differ from the parent states by changing one electron from an nl to an $n'l'$ single-particle state. In Eq. (12) $P(\lambda)$ is the probability of the parent state, $f(\lambda\rightarrow\lambda')$ is the oscillator strength of the transition, and ΔE is the energy difference. The last term in Eq. (12) is the average oscillator strength for an $nl-n'l'$ transition array given by

$$f_{nl\rightarrow n'l'}(a)=\sum_{\lambda,\lambda'} P(\lambda)f(\lambda\rightarrow\lambda')\ , \tag{13}$$

the values of which are shown in column 7 in Table III. The oscillator strength for an $nl-n'l'$ transition predicted by the AA model is given by

$$f_{nl\rightarrow n'l'}(aa)=\tfrac{2}{3}\Delta E_{nl\rightarrow n'l'}(aa)g_{nl}\times\frac{l_>}{2l+1}\,|\,D(nl\rightarrow n'l')\,|^2\ , \tag{14}$$

where q_{nl} is the occupation number of the shell nl as given by Eq. (1) and D stands for the dipole radial integral. The AA oscillator strengths are shown in column 6 in Table III. It should be noted that we use the same dipole radial integrals needed for the AA and the detailed $J-J'$ oscillator strengths by using the AA radial wave functions, so the difference between the $f(aa)$ and $f(a)$ quantities is due only to the statistical distribution of the parent states and to the transition energies. In columns 4 and 5 we also give the second and third moments of the distribution of lines within an array given by the formula for the kth moments

TABLE III. Energies, variances in eV and oscillator strengths for transition arrays in bromine plasma at $kT=270$ eV and at $\rho=2.6\times10^{-2}$ g/cm^3. The numbers in square brackets are exponents of 10.

Array	$\Delta E(aa)$	$\Delta E(a)$	$[\Delta^2]^{1/2}$	$[\Delta^3]^{1/3}$	$f(aa)$	$f(a)$
$2s$-$3p$	1.834[3]	1.831[3]	5.051[1]	4.769[1]	5.780[−1]	6.145[−1]
$2s$-$4p$	2.363[3]	2.375[3]	7.256[1]	6.309[1]	1.557[−1]	1.639[−1]
$2s$-$5p$	2.600[3]	2.621[3]	8.379[1]	7.090[1]	6.459[−2]	6.787[−2]
$2p$-$3s$	1.627[3]	1.623[3]	6.463[1]	5.440[1]	8.300[−2]	8.444[−2]
$2p$-$3d$	1.744[3]	1.768[3]	5.346[1]	4.507[1]	2.937	3.095
$2p$-$4s$	2.185[3]	2.195[3]	8.562[1]	7.000[1]	1.866[−2]	1.911[−2]
$2p$-$4d$	2.231[3]	2.249[3]	8.107[1]	6.623[1]	6.345[−1]	6.548[−1]
$2p$-$5s$	2.433[3]	2.451[3]	9.625[1]	7.784[1]	7.199[−3]	7.380[−3]
$2p$-$5d$	2.456[3]	2.477[3]	9.376[1]	7.573[1]	2.447[−1]	2.516[−1]

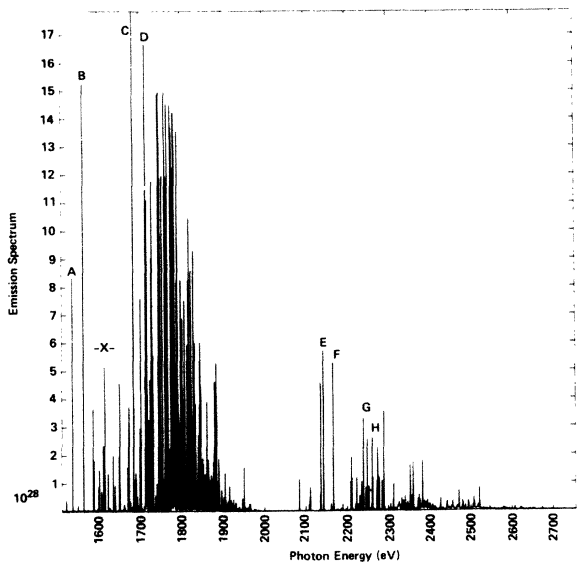

FIG. 8. Same as Fig. 6 at $kT=250$ eV and $\rho=1.667\times10^{-2}$ g/cm^3. The X indicates the region of the F-like $2p$-$3s$ transitions.

$$\Delta^k(nl\rightarrow n'l')=\sum_{\lambda,\lambda'}P(\lambda)f(\lambda\rightarrow\lambda')\times[\Delta E(\lambda\rightarrow\lambda)-\Delta E_{nl\rightarrow n'l'}(a)]^k\times f^{-1}_{nl\rightarrow n'l'}(a)\ . \quad (15)$$

The fact that the third moments are not small indicates that the line distributions are not symmetric around the average as in a simple Gaussian model.

The emission spectrum of the laser-produced bromine plasma in another temperature-density region, estimated to be 710 eV and 3×10^{21} electrons/cm^3, respectively, is shown in Fig. 7. This density corresponds to 1.667×10^{-2} g/cm^3 and to obtain mainly neon- and fluorine-like states our LTE model had to assume 250 eV temperature. Our computed emission spectrum for this case is shown in Fig. 8. Again, the transition energies of the prominent neon-like lines show reasonable agreement between theory and experiment, but the line intensities are noticeably different. Also, in the region of 1700—1900 eV photon energy our LTE calculation shows more strong lines than the experiment. We attribute this difference again to the difference between the LTE model and non-LTE experimental conditions.

In summary, the algorithm described in this paper is applicable to the computation of LTE spectra for partially filled L shells (and, of course, K shells). Further improvements in the physics of the model, such as configuration interaction may perturb the relative strengths and position of the spectral lines, but does not change their number. The same principle could be applied to the case of partially filled M or higher shells, but in those cases the number of spectral lines could very well become astronomical. For this reason we believe that our model provides sufficiently accurate predictions for LTE K- and L-shell spectra. We are aware that LTE conditions are difficult to achieve in laboratory conditions; nevertheless, we hope that spectra from LTE plasmas will be available in the not too distant future.

ACKNOWLEDGMENTS

The authors are grateful to Dr. T. Phillips and to R. Walling for several useful discussions, and we thank them and their coauthors of Ref. 16 for their permission to reproduce Figs. 1 and 7. Work performed under the auspices of the U.S. Department of Energy by Lawrence Livermore National Laboratory under Contract No. W-7405-Eng-48.

[1]See Harris Mayer, Los Alamos Scientific Laboratory Report No. 647, 1947 (unpublished).
[2]E. Nardi and Z. Zinamon, Phys. Rev. A **20**, 1197 (1979).
[3]B. F. Rozsnyai, J. Quant. Spectrosc. Radiat. Transfer **27**, 211 (1981).
[4]S. A. Moszkowski, Prog. Theor. Phys. **28**, 1 (1962).
[5]C. Bauche-Arnoult, J. Bauche, and M. Klapisch, Phys. Rev. A **10**, 242 (1979).
[6]C. Bauche-Arnoult, J. Bauche, and M. Klapisch, Phys. Rev. A **25**, 264 (1982).
[7]J. Bauche, C. Bauche-Arnoult, E. Luc-Koenig, J. F. Wyart, and M. Klapisch, Phys. Rev. A **28**, 829 (1983).
[8]B. F. Rozsnyai, Phys. Rev. **145**, 1137 (1972).
[9]L. Hedin and B. I. Lundqvist, J. Phys. C **4**, 2064 (1971).
[10]M. F. Argo and W. F. Huebner, J. Quant. Spectrosc. Radiat. Transfer **16**, 1091 (1976).
[11]A. Goldberg and B. F. Rozsnyai, *Radiative Properties of Hot Dense Matter* (World Scientific, Singapore, 1985), p. 423.
[12]B. F. Rozsnyai, J. Quant. Spectrosc. Radiat. Transfer **17**, 77 (1977).
[13]B. F. Rozsnyai, J. Quant. Spectrosc. Radiat. Transfer **19**, 641 (1978).
[14]B. F. Rozsnyai, J. Quant. Spectrosc. Radiat. Transfer **13**, 1285 (1973).
[15]B. F. Rozsnyai, J. Quant. Spectrosc. Radiat. Transfer **22**, 337 (1979).
[16]J. Bailey, R. E. Stewart, J. D. Kilkenney, R. S. Walling, T. Phillips, R. J. Fortner, and R. W. Lee, J. Phys. B (to be published).

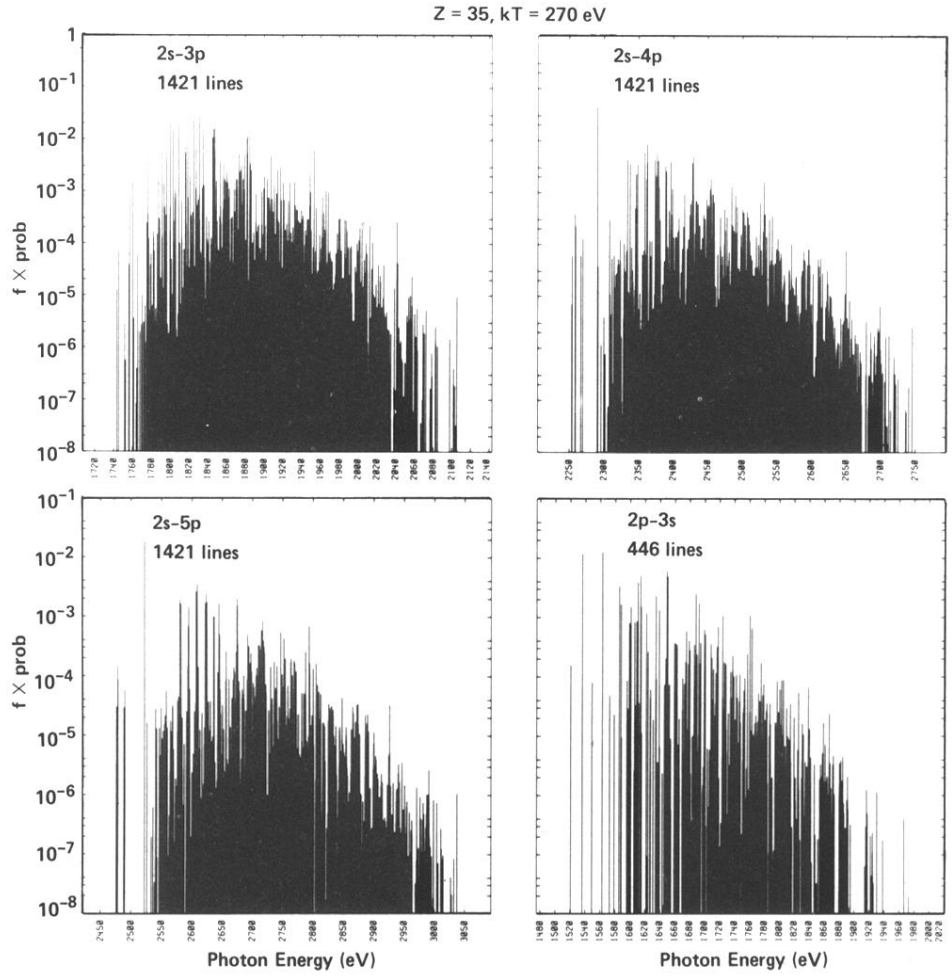

FIG. 2. Computer output for the $2s$-$3p$, $2s$-$4p$, $2s$-$5p$, and $2p$-$3s$ transition arrays vs photon energy in eV for bromine plasma at $kT=270$ eV and at $\rho=2.6\times10^{-2}$ g/cm^3. The vertical scale is for the oscillator strengths multiplied by the probability of the parent state.

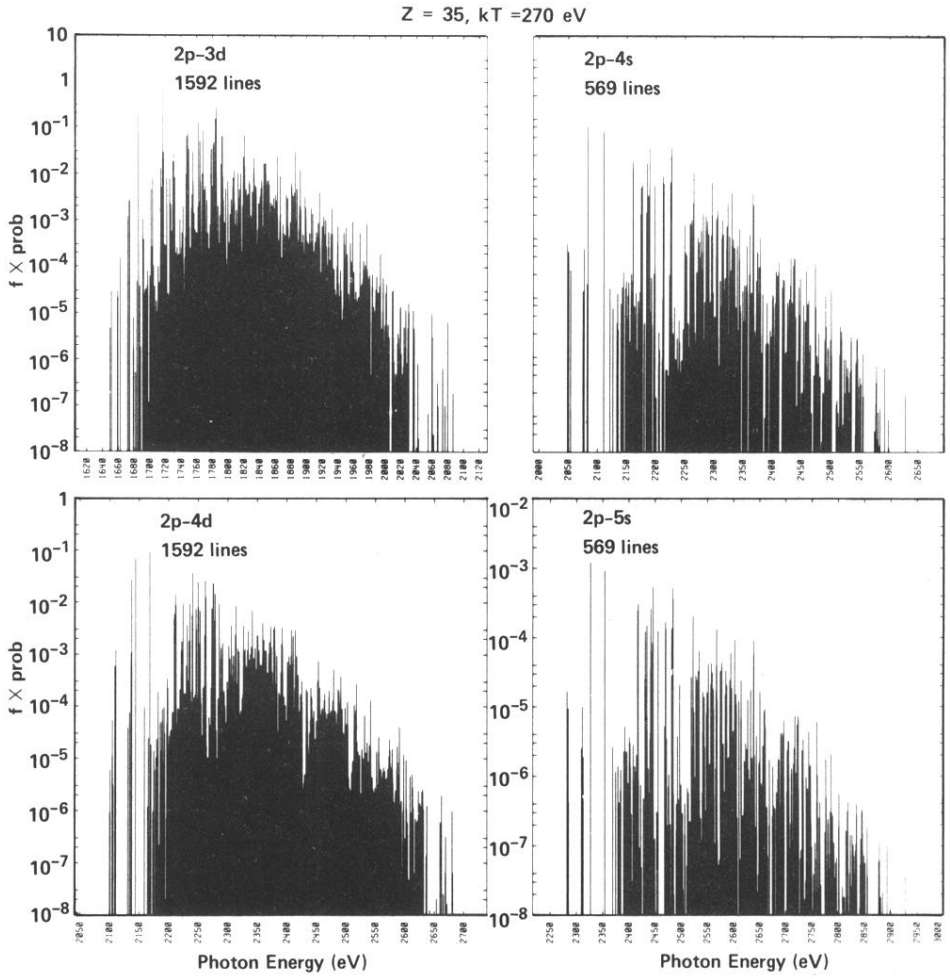

FIG. 3. Same as Fig. 2 for the $2p$-$3d$, $2p$-$4s$, $2p$-$4d$, and $2p$-$5s$ arrays.